Electroencephalographic brain dynamics following visual targets requiring manual responses

Scott Makeig* (1), Arnaud Delorme (1), Marissa Westerfield (4),
Tzyy-Ping Jung (1), Jeanne Townsend (4),
Eric Courchesne (3,4) and
Terrence J. Sejnowski (1,2)

Revision of March 12, 2004

(1) Swartz Center for Computational Neuroscience
Institute for Neural Computation
University of California San Diego
La Jolla CA 92093-0961
(858) 458-1927 x11 office
(858) 458-1847 fax
smakeig@ucsd.edu

(2) Howard Hughes Medical Institute
Computational Neurobiology Laboratory
The Salk Institute for Biological Studies
La Jolla, CA 92037

(3) Children's Hospital Research Center
San Diego CA

(4) Department of Neurosciences
University of California San Diego
La Jolla, CA 92093

**To whom correspondence should be addressed.*

Abbreviated Title: **EEG Dynamics Following Visual Targets** (33 characters)

The manuscript includes 49 double-spaced text pages, 13 figures, 1 animation, and no tables.

Acknowledgments: This report was supported by The Swartz Foundation, the National Institutes of Health (NINDS NS34155 and NIMH MH36840), and the Howard Hughes Medical Institute. Thanks to Stefan Debener for detailed comments.

Keywords: EEG, electroencephalogram, ERP, P300, ERSP, motor, cingulate, ICA, theta, alpha, mu, beta, coherence, phase resetting, visual.

Abstract

Background: Scalp-recorded electroencephalographic (EEG) signals produced by partial synchronization of cortical field activity mix locally synchronous electrical activities of many cortical areas. Analysis of event-related EEG signals typically assumes that post-stimulus potentials emerge out of a flat baseline. Signals associated with a particular type of cognitive event are then assessed by averaging data from each scalp channel across trials, producing averaged event-related potentials (ERPs). ERP averaging, however, filters out much of the information about cortical dynamics available in the unaveraged data trials.

Methodology/Principal Findings: Here, we studied the dynamics of cortical electrical activity during detecting and manually responding to visual targets, viewing signals retained in ERP averages not as responses of an otherwise silent system but as resulting from event-related alterations in ongoing EEG processes. We applied infomax independent component analysis (ICA) to parse the dynamics of the unaveraged 31-channel EEG signals into maximally independent processes, then clustered the resulting processes across subjects by similarities in their scalp maps and activity power spectra, identifying nine classes of EEG processes with distinct spatial distributions and event-related dynamics. Coupled two-cycle post-motor theta bursts followed button presses in frontal midline and somatomotor clusters, while the broad post-motor 'P300' positivity summed distinct contributions from several classes of frontal, parietal and occipital processes.

Conclusions/Significance: The observed event-related changes in local field activities, within and between cortical areas, may serve to modulate the strength of spike-based communication between cortical areas to update attention, expectancy, memory, and motor preparation during and after target recognition and speeded responding.

Introduction

The waking brain updates and fulfills intentions through brain processes that operate within and across multiple brain areas to integrate perception, association and action. Fulfillment of intentions is facilitated by features of these and other processes that support informed anticipation of and selective attention to events and their probable consequences. The dynamics of ongoing EEG activity recorded from the human scalp differ markedly with state of attention and intention (Makeig and Inlow, 1993; Worden et al., 2000), yet most event-related EEG research has assumed that the effects of events on EEG signals emerge out of a flat baseline, as in the typical averaged event-related potential (ERP). The electrophysiological consequences of stimulus events spread quickly in the brain. By 50-150 ms, sensory stimulus information is widely distributed (Hupe et al., 2001), perturbing ongoing patterns of local field activity in many brain areas (Klopp et al., 2000). There is little chance, therefore, that any but still earlier event-related ERP features occur within single brain areas.

The adequacy of time-domain ERP averaging for modeling macroscopic brain dynamics also depends on the assumption that the cortical sources of EEG activity contributing and not contributing to average ERP waveforms are somehow distinct. The scalp topographies of unaveraged EEG and averaged ERP data may, however, be quite similar (Makeig et al., 2002a), strongly suggesting that areas contributing to ongoing EEG signals may also contribute to ERP averages. EEG processes not contributing to response averages may also be affected by experimental events, and several types of dynamic EEG response processes are not reflected in ERP averages (Pfurtscheller and Aranibar, 1977; Makeig, 1993; Makeig et al., 2002a). A more comprehensive model of event-related brain dynamics is therefore needed to capture features of EEG signals that index the dynamic interplay between spatially coherent brain processes supporting anticipation of, attention towards, associations to, and behavioral responses following experimental events.

The above considerations suggest that event-related EEG dynamics may be better modeled as coordinated event-related perturbations in the statistics of multiple, intermittently active local field processes. Since the volume-conducted scalp projections of such processes generally overlap, they cannot be separately identified in the scalp-recorded data. An alternate approach we adopt here is to separate their contributions by using distinct differences in their time courses (Makeig et al., 1996a, 1997; Jung et al., 2001a).

Following stimuli belonging to an anticipated but infrequently-presented category, the averaged ERP is dominated by a broad vertex-positive peak often called P300 after its earliest appearance in auditory responses (Sutton, et al., 1965; for review, see Soltani et al., 2001). Results of ERP (Ruchkin et al., 1990) and brain lesion studies (Halgren et al., 1980; Knight et al., 1989), and functional imaging experiments (Ford et al., 1994; Ebmeier et al., 1995; Ardekani et al., 2002) strongly suggest that 'P300' is actually a late positive-going response complex (LPC) that sums effects of local field perturbations in several brain regions. A more inclusive model of the event-related EEG brain dynamics occurring in such data should model, therefore, how target stimulus presentations and subject motor responses perturb the dynamics of ongoing EEG signals both within and across single subjects. Here, we present such a model.

Methods

Task design. Event-related brain potentials (ERPs) were recorded from subjects who attended to randomized sequences of filled disks appearing briefly inside one of five empty squares that were constantly displayed 0.8 cm above a central fixation cross (Fig. 1) following Townsend and Courchesne (1994). The 1.6-cm square outlines were displayed on a black background at horizontal visual angles of 0°, ±2.7º and ±5.5º from fixation. During each 76-s block of trials, one of the five outlines was colored green and the other four blue. The green square marked the location to be attended. This location was varied in random counterbalanced order across blocks. In each block, 100 stimuli (filled white disks) were displayed for 117 ms within one of the five empty squares in a pseudo-random sequence with inter-stimulus intervals (ISIs) of 250 to 1000 ms (in four equiprobable 250-ms steps).

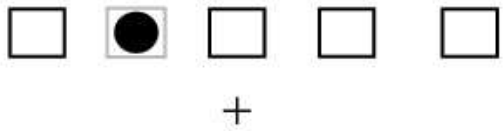

Figure 1. Task display. *Subjects fixated a cross above which five boxes were constantly displayed. In each 76-s task block, one of these (grey box) was colored differently. The location of this covertly attended box varied pseudo-randomly across blocks. A series of disks were presented briefly in any of the five boxes in a random order. Subjects were asked to respond with a thumb button press as quickly as possible whenever a disk appeared in the attended box.*

Subjects and task. Fifteen right-handed volunteers (ages 19 to 53 years, mean 30; 12 male, 3 female) with normal or corrected to normal vision participated in the experiment. Subjects were instructed to maintain fixation on the central cross while responding only to stimuli presented in the green-colored (attended) square. Subjects were required to press a thumb button held in their dominant right hand as quickly as possible following stimuli presented in the attended location (Fig. 1). Thirty blocks of trials were collected from each subject, yielding 120 target and 480 non-target trials at each location. Subjects were given ~2-min breaks between blocks.

EEG recordings. EEG data were collected from 29 scalp electrodes mounted in a standard electrode cap (Electrocap, Inc.) at locations based on a modified International 10-20 System, and from two periocular electrodes placed below the right eye and at the left outer canthus. All channels were referenced to the right mastoid with input impedance less than 5kΩ. Data were sampled at 512 Hz with an analog pass band of 0.01-50 Hz. To further minimize line noise artifacts, responses were digitally low pass filtered below 40 Hz prior to analysis. After rejecting trials containing electrooculographic (EOG) potentials larger than 70 μV or amplifier blocking, brain responses to stimuli presented at each location in each attention condition were stored separately. Responses to target stimuli were analyzed only when (as in nearly all cases) subjects responded 150-1000 ms after target onset. The few targets followed by no such button press were not considered in the present analysis.

Previous analysis. Analysis of average ERP and some single-trial data from these experiments have been reported previously. Makeig et al. (1999a) first reported ICA decompositions of late (P300) target responses in a 5×5 matrix of grand-mean visual stimulus ERPs from these experiments (5 stimulus locations by 5 attended locations). They reported three maximally independent ERP components of

interest which they labeled P3f, P3b and Pmp. Makeig et al. (1999b) applied the same multiple-ERP analysis to the first 250 ms period following stimulus onsets and demonstrated distinct contributions to the N1 ERP peak were generated in the right hemisphere 9 ms earlier, on average, than in the left. ICA separates component processes mixed in scalp data based on their relative temporal independence, which should be maximally expressed in the *unaveraged* data. Systematic application of ICA to unaveraged data from these experiments was first demonstrated for non-target stimulus trials (Makeig et al., 2002a). In that analysis, a 100-ms post-stimulus period (150-250 ms after stimulus onset) was extracted from each of the over 3,000 trials for each subject and these data were concatenated and decomposed by ICA. Some information about the target stimulus trials was also presented in Jung et al. (2001b). Here we report results of comparing ICA decompositions of roughly 600 1-s target-response trials from each of 15 subjects.

Independent component analysis. Infomax ICA (Bell & Sejnowski, 1995; Makeig et al., 1996a) is one of a family of algorithms that exploit temporal independence to perform blind separation of underlying data sources. Lee et al. (1999a) have shown that these algorithms have a common information theoretic basis, differing chiefly in the form of distribution assumed for the sources, which may not be critical (Amari, 1998). Infomax ICA finds, by natural gradient ascent, a square 'unmixing' matrix that maximizes the joint entropy (Cover & Thomas, 1991) of a nonlinearly transformed ensemble of zero-mean input data vectors. Maximizing joint entropy implies, under reasonable assumptions (Bell & Sejnowski, 1995), minimizing mutual information among the component activities. This means that information about the simultaneous activity values of any number of the components gives minimum information about the concurrent activity values of any other components.

Independent component activities are minimally correlated, both in standard second-order and in higher-order senses. That is, they each appear to ICA to be 'free-running' and in this sense act as separate sources of information in the data. The power of infomax source separation in a growing range of signal processing applications derives from its basic aim to identify information sources in data, in contrast to previous root-mean square estimation methods that aim simply to model data variance (Jung et al., 2001a). Natural-gradient logistic infomax ICA in the automated form we use here (runica, Makeig et al., 1977), can accurately decompose mixtures of component processes having symmetric or skewed distributions without requiring nonlinearities specifically tailored to them, and can be usefully applied to EEG data from 100 or more channels. The number of time points required for training may be as few as several times the number of unmixing weights (usually the square of the number of channels), though using more (clean) training data is preferable. In turn, the number of channels must be at least equal to (and preferably larger than) the number of interpretable components to be separated (Makeig et al., 1999a).

The success of ICA applied to EEG data is strictly determined by the degree to which EEG dynamics fit the ICA model. The first requirement, that the underlying sources mix linearly in the electrode recordings, is assured by the biophysics of volume conduction at EEG frequencies (Nunez, 1981). The assumption of relative spatial stationarity of EEG sources is compatible, at least, with evidence of brain modularity from anatomy and functional imaging. The assumption of relative independence of the source signals is compatible with physiological models that emphasize local, short-range intracortical and radial thalamocortical coupling in the generation of local electrical synchronies in the EEG range (Salinas and Sejnowski, 2003).

The ultimate validity of the assumptions above in any data set cannot be guaranteed a priori. The consistency and physiologic plausibility of the results of ICA decompositions, such as we present here, including their often tight linkage to behavioral and cognitive variables, are strong indirect evidence for the workability of the assumptions and of the ICA model. Direct physiological testing of the model and its physiologic assumptions will require development of multiscale recording methods. Meanwhile, yet more flexible (but also more intricate) ICA models of EEG activity are possible (e.g., Anemueller et al., 2003). It remains to be seen, however, whether the information gain offered by such models exceeds the loss of statistical power associated with their higher complexity.

As first demonstrated by simulations (Makeig et al., 1996b), when training data consist of a mixture of fewer large source components than channels, plus many more small source components, as might be expected in actual EEG data, large source components are accurately separated into separate output components, with the remaining output components consisting of mixtures of smaller source components. In this sense, performance of the infomax ICA algorithm degrades gracefully as the amount of 'noise' in the data increases. For more details about applying ICA to ERP and EEG data, see Makeig et al. (1999a, 2002a) and Jung et al. (2000a, 2000b).

Here, the runica algorithm (available for download with the EEGLAB toolbox of Delorme and Makeig (2004a) from *www.sccn.ucsd.edu/eeglab*) was applied to sets of 400 to 600 single 1-s trials (31 channels, 256 time points) time locked from -200 ms before to 800 ms after onsets of target stimuli presented at any of the five stimulus locations (Fig. 1). Target trials in which the subject did not respond with a button press (fewer than 5%) were removed from the data. Learning batch size was 50. Initial learning rate began near 0.0004, and was gradually reduced to 10-6 during 50-150 training iterations that required about 30 min of computer time. Results of the analysis were relatively insensitive to the exact choice of learning rate or batch size. Reducing the stopping weight change from 10-6 to 10-7 did not appear to change the resulting decompositions qualitatively, although when decomposing data from many more channels we have since noted an advantage to continuing to train until weight change falls below 10-7.

Component clustering. Commonly in ERP research, neural activity expressed in periocular data channels is ignored for fear of mislabeling eye-activity artifacts as brain activity. Some ICA components of EEG records can be clearly identified as accounting primarily for eye movements, line or muscle noise, or other artifacts through their characteristic scalp maps and activity time courses (Makeig et al., 1996a; Jung et al., 2000a, 2000b). Subtracting the projections of artifactual components from averaged or single trial data can eliminate or strongly reduce these artifacts while preserving the remaining non-artifactual EEG phenomena in all of the data channels. ICA thus makes it possible, for the first time, to examine periocular EEG activity apart from eye movements.

Here, the total of 31×15 = 465 component maps and mean activity log spectra from the 15 subjects were clustered by applying a modified Mahalanobis distance measure (Enghoff, 1998; see Appendix, Jung et al., 2001b) to vectors coding differences in the component 31-channel (x, y) map gradients and activity log spectra after reduction to 12 and 5 dimensions respectively by principal component analysis (PCA). Cluster membership was in a few cases then further adjusted by eye for uniformity. Clustering based on scalp map gradients and activity spectra, as reported here, is one of several possible component clustering approaches, whose relative advantages have not yet been explored.

Event-related spectral dynamics. To examine stimulus- and response-induced changes in the EEG spectrum, we computed event-related spectral perturbation (ERSP) transforms (Makeig, 1993) for each channel and each clustered independent data component using the publicly available EEGLAB toolbox (Delorme and Makeig, 2004a, 2004b). ERSPs show changes (in dB) from baseline in spectral power across a broad frequency range (here, 3-50 Hz). The time/frequency analysis used Hanning-windowed sinusoidal wavelets of 3 cycles at 3 Hz, rising linearly to about 15 cycles at 30 Hz. This modified wavelet transform was selected to optimize the trade-off between temporal resolution at lower frequencies and stability at higher frequencies.

Constructing surrogate data sets by shuffling the data epoch sub-windows used to construct the time-locked spectral average allowed choosing an initial within-subject significance cutoff (not corrected for multiple comparisons) of $p<.01$. To construct between-subject mean ERSPs, we used binomial statistics to select as a significance cutoff a minimum number of subjects required to have significant differences (in the same direction) from baseline at a given time/frequency point ($p<.0001$). ERSP transforms of the data were computed at each channel and then for each clustered data component. To test for partial phase-locking (i.e., non-random phase relationship) between EEG processes and the occurrence of experimental events across trials, we used inter-trial phase coherence (ITC) (Makeig et al., 2002a).

To test the presence of non-random phase relationships (possibly including fixed delays) between activities in different (maximally) independent components, we performed event-related phase coherence (ERCOH) analysis (Makeig et al., 2002a; Delorme et al., 2003), again with a single-subject bootstrap significance threshold of $p<.01$ (uncorrected), between pairs of independent components (from the same subject) included in each pair of independent component clusters (defined below). To exclude the possibility that the observed phase linkages arose only from common phase-locking of the portion of the single-trial data constituting the ERP, we also subtracted the concurrent mean ERP from each trial before computing phase coherence. Functions to compute and plot the time/frequency measures used here are also available in the EEGLAB toolbox.

Equivalent dipole modeling. Both simple anatomic considerations and observed results of ICA decomposition suggest that cortical EEG sources may be usefully modeled as patches of cortex with partially synchronous local field activities. In brief, the high local coupling density of both excitatory and particularly, inhibitory neurons in cortex means that local field potentials sufficiently synchronous to create measurable EEG signals should tend to extend through a compact spatial domain – roughly speaking, a patch of cortex of unspecified extent. Through volume conduction, partially synchronous activities within source cortical source patches produce far-field potentials throughout the brain and on the scalp. The distribution of the scalp electrical field produced by such a source patch is nearly identical to that of a small dipolar potential element whose geometry is like a tiny 'flashlight battery,' oriented perpendicular to the cortical surface. This 'battery' is termed the equivalent dipole for the cortical source.

Here, we used a relatively simple and well-known method for fitting the positions and orientations of equivalent dipoles in a four-shell spherical head model for each component (BESA; Megis Software, Munich). To reduce the time required to process the 485 component maps, we used a version (3.0) of the BESA software that allowed batch processing to fit single-dipole models to each component scalp map. (A *dipfit* tool set of R. Oostenveld, producing equivalent results, is now available at *sccn.ucsd.edu/eeglab/dipfit.html*). Some bilaterally symmetric component maps were better fit with

symmetric dual-dipole models. The successful fits of single-dipole models for many of the clustered components is compatible with their generation within a single, compact patch of cortex, while bilateral dual-dipole models are compatible with tightly coupled oscillatory activity (without net phase delay) in two bilaterally symmetric cortical patches densely connected via corpus callosum and/or common subcortical drive.

To distinguish the relative regional locations of the component clusters, the scalp maps for the individual components in each cluster were first oriented similarly (e.g., so as to all be positively correlated), normalized, and then averaged. These cluster mean maps were then fit with single-dipole models to roughly illustrate the regional distinctions between the sources of the component clusters. Finally, the cluster-mean dipoles and event-related time/frequency information measured by ERSP, ITC and ERCOH analysis of all the single trials were visualized together in three dimensions using an animated display developed by Delorme et al. (2003).

Results

The ICA analysis method provides a complete decomposition of the single-trial (or continuous) EEG data, separating the data into distinct information sources. As the results presented below show, the amount of information about cortical dynamics provided by this method is large. Here, we detail for the first time dynamics occurring within single trials of the classes of maximally independent EEG processes whose event-related activities contribute to visual target responses. To help the reader digest the many details of interest this analysis revealed, we separate our presentation of the results and their interpretation into five sections, followed by a general Discussion.

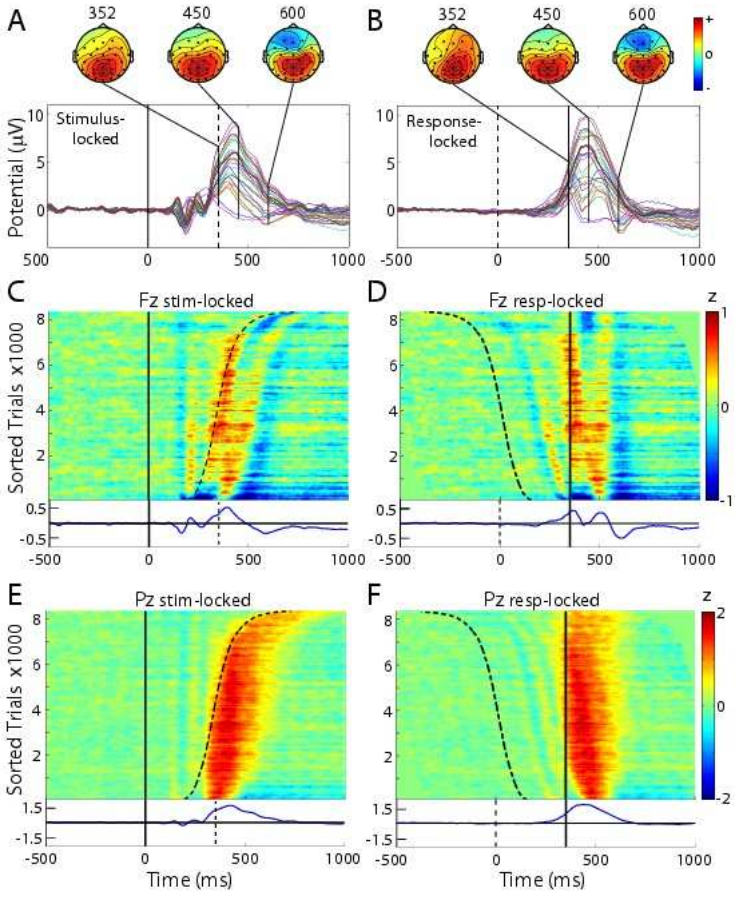

Figure 2. Grand mean and response-time ordered single-trial responses at sites Fz and Pz. *(Left) Stimulus-locked grand mean and (Right) response-locked grand mean responses to target stimuli. (A-B) Grand mean responses at all 29 scalp channels (colored traces), plus scalp maps at indicated latencies. (C-F) Grand moving-mean single-trial responses from all 15 subjects, at fronto-central site Fz (C,D) and at central parietal site Pz (E,F), plotted in ERP-image format and sorted by subject reaction time (curving dashed trace in left column; vertical solid line in right column, plotted at the mean subject-median response time of 352 ms). ERP-image units: z = μV divided by RMS μV in the (-1000 ms to 0 ms) channel baseline EEG of the same subject after removal of eye and muscle artifact components from the data. Vertical smoothing window: 300 trials. Grand mean normalized responses are shown below each image.*

1. Response dynamics of the scalp recordings: ERPs and ERP images. To orient readers used to analyses of the raw scalp-channel data, we first present conventional ERP results at selected channels. As we previously reported, in these experiments performance level was high; more than 95% of targets were followed by a button press within the allotted (150-1000 ms) response window. Mean subject-median reaction time (RT) was 352 ms. The ERP time locked to onsets of target stimulus followed by a subject button press contained the expected late positive complex or 'P300' positivity following early stimulus-locked peaks conventionally termed P1, N1, P2 and N2 (see Fig. 2A). The scalp topography of the late positive complex varied continuously through its extent (Fig. 2A, *scalp maps*).

In the grand average of the same epochs, each time-locked to the subject response (Fig. 2B), the early response-locked peaks became smeared out, and the P300 and succeeding negative dip more concentrated. In two-dimensional 'ERP-image' plots of the 8,413 single trials from all 15 subjects (Fig. 2C-F), potential fluctuations in single trials are shown as color-coded horizontal lines, here normalized by subject baseline variability, then sorted (across all trials) by reaction time (RT) and smoothed (vertically) with a 300-trial moving average. The ERP images clearly show that the early visual response peaks at central posterior site Pz (Fig. 2E) were time-locked to stimulus onset, while the late positivity at Pz immediately followed the button press (compare Fig. 2E and 2F) except in trials with quickest RTs. Over half of these were contributed by two fast-responding subjects whose responses, unlike those of the other 13 subjects, preceded P300 onset.

At frontocentral channel Fz, however, the late positivity in the stimulus-locked grand average (Fig. 2C, bottom) was largely composed of two response-locked positive peaks, separated by 200 ms, that together with intervening and flanking negativities could be partially modeled by a two-cycle, 5-Hz wavelet (Fig. 2D). The single 'P300' peak at Fz in the stimulus-locked ERP (Fig. 2A) 'smears out' the two-cycle pattern that is captured clearly in the response-locked average (Fig. 2B,D), while highlighting a concurrent, broader, and possibly stimulus-locked positivity in faster-RT trials (Fig. 2C).

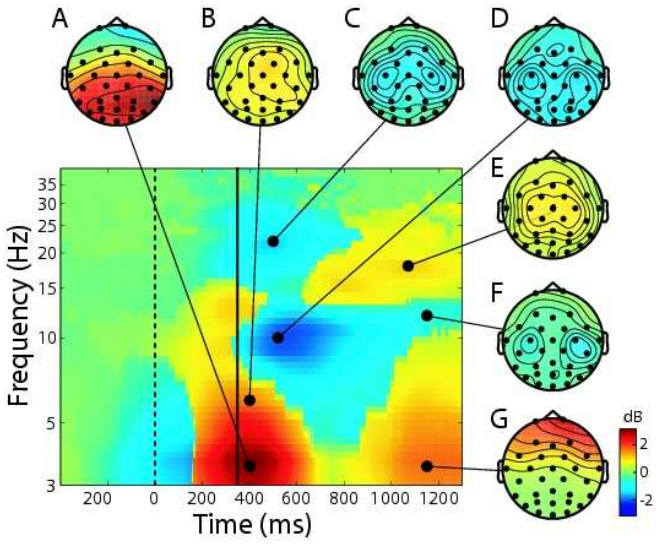

Figure 3. Changes in mean scalp spectral power time-locked to the subject response *(solid vertical line, adjusted to the mean subject median, 387 ms). Color scale: dB change from pre-stimulus baseline. Image shows signed-RMS power changes across all 29 scalp channels prior to removal of all but the largest eye artifacts. Scalp maps show the scalp topography of the spectral power change in dB relative to baseline. Note (A,B) the broad posterior low theta and anterior higher-theta band maxima at the button press, (C,D,F) the bilateral central alpha and beta blocking, (E) the central-lateral post-response beta increase, and (G) the increase in low-frequency eye artifacts at the end of the record.*

Event-related spectral perturbations. Figure 3 summarizes the grand mean time course of changes from pre-stimulus baseline in log spectral EEG power at all the scalp channels time locked to button presses (solid vertical line) across the EEG frequency range. During and just prior to the button press, a circa 3-dB increase in low theta band power peaked (red area) near 4 Hz in bilateral central and posterior cortex.

This increase remained significant ($p < .01$) for 14 of the 15 subjects even after the subject-mean ERP was subtracted from each trial (not shown).

A concurrent but weaker theta power increase near 6 Hz (Fig. 3B) was maximal at frontocentral and parietal scalp sites. The theta increase at these sites was accompanied by blocking of circa 10-Hz and 22-Hz mu activity, maximal at the left and right central scalp but also widespread over posterior scalp (Fig. 3C,D,F). Following the button press, a late central bilateral increase in beta activity (maximal at 16-18 Hz) appeared (Fig. 3E). Fig. 3 was computed prior to performing ICA and removing eye movement artifacts. The diffuse, far frontal increase in 3-10 Hz activity that began 500 ms after the button press (Fig. 3G) doubtless reflects increased subject eye activity following the target response.

2. ICA decompositions. Conventionally, characterizing the sources of ERP (Fig. 2) or ERSP (Fig. 3) processes is thought to be difficult because the scalp sensors are relatively far from the actual brain sources and therefore each sums the volume-conducted activities of several source areas. Moreover, the biophysical inverse problem of determining the potential source distribution from a given scalp map is in general severely under constrained. Nonetheless, infomax ICA, applied (by runica) to the concatenated single trials for each subject, after removing trials containing out-of-bounds or uncharacteristic artifacts, decomposed the whole set of concatenated EEG signals into 31 spatially-fixed, temporally maximally independent component processes, and the scalp maps associated with many of these processes resembled the scalp projections of synchronous activity in either one or sometimes two near-bilaterally symmetric cortical patches.

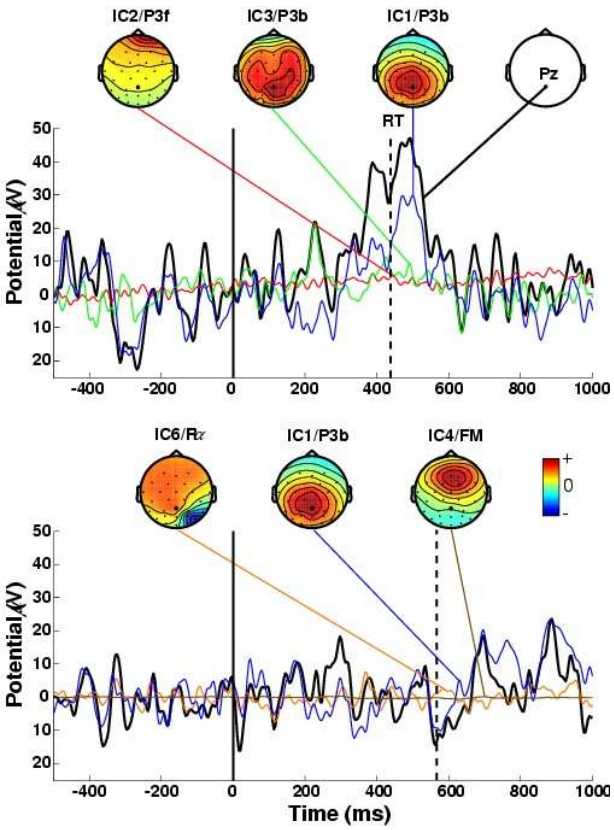

Figure 4. Independent component decompositions for two single trials*. (Black traces) Two of 561 single target-response trials from one subject at scalp site Pz (upper right scalp map). (solid vertical lines) Stimulus onsets, (dashed vertical lines), button presses. A prominent late positivity occurred in the upper trial. All 561 1-sec, 31-channel EEG epochs time locked to target stimuli were concatenated and decomposed by infomax ICA, yielding 31 maximally independent data components. Colored traces show the projections (in μV) to this scalp channel of the three (non-artifact) independent components contributing the largest variance to each post-response data window, linked to (individually scaled) maps of their scalp topographies. Component numbers (IC1-IC6), as ranked by total EEG variance accounted for, and cluster affiliations (P3f, P3b, FM, P3b, Rα) are indicated above the scalp maps. Note differences in the time courses of IC1.*

Component contributions to the single-trial EEG signals. Figure 4 shows two single trials at site Pz (*black traces*) from one subject after removal of six eye and muscle artifact components. Projected

activities of the three independent components most strongly contributing to each trial are shown at thin colored traces and accompanying scalp maps. Since infomax ICA provides a complete linear decomposition, the observed data (*black traces*) are in each case the sum of the remaining 31 - 6 = 25 component projections, including the 3 component projections shown. In the upper trial, and typically, the single-trial P300 at Pz was accounted by ICA as summing contributions of at least two independent EEG processes. Component IC1 for this subject (ranked first by amount of total EEG variance accounted for) was eventually included in the parietal 'P3b' component cluster (described below) on the basis of its scalp map and activity power spectrum.

While component IC1 accounted for the largest part of the P300 peak in the upper trial, in the lower trial the same IC1 process showed mixed low alpha and beta activity with a smaller post-motor response positivity. Note the positive post-response contribution of IC1 in this trial (*thin blue trace*) was sometimes larger than the observed positivity in the whole channel data (*thick black trace*). At these times, some of the other 24 components contributed negative potentials to the signal at this scalp channel, partially canceling the IC1 positivity in the recorded data. Thus ICA, applied to the continuous or concatenated single-trial data, may actually recover more of the actual projected signals than are available in the single-channel data.

Independent component clusters. Cluster analysis, applied to the normalized scalp topographies and power spectra of all 465 components from the 15 subjects (see Methods), identified at least 13 clusters of components having similar power spectra and scalp projections. These component clusters also showed functionally distinct activity patterns. Four distinct component clusters (not shown) accounted for eye blinks, horizontal eye movements and left and right temporal muscle noises respectively. These were effectively removed from the activity of the other component clusters by the ICA decomposition, and are not further considered here.

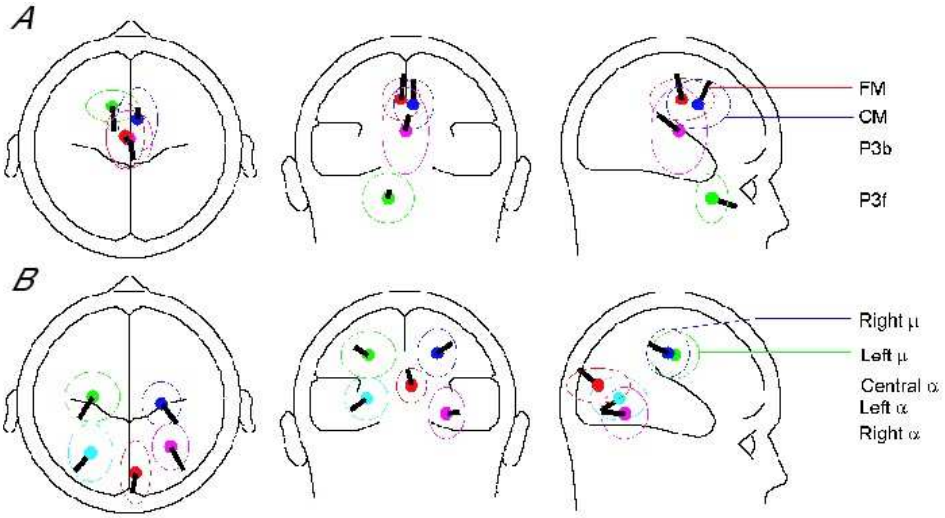

Figure 5. Mean component cluster equivalent-dipole locations. *The mean scalp map for each of the nine component clusters could be well fit by a single equivalent dipole (mean residual variance, 4.8%). The figure shows the locations and orientations of these dipoles, as determined by BESA, plotted on the spherical head model, with ellipses showing the spatial standard deviation of the locations of the equivalent dipoles for the individual components in the cluster.*

Equivalent dipole locations. Figure 5 shows the results of modeling the grand mean scalp maps for each of the nine independent component clusters as the projection of an equivalent dipole. Residual scalp map variances unaccounted for by these models were relatively small (range, 0.87% to 9.55%; mean, 4.93%), though the equivalent dipole locations for the individual clustered components were not all tightly clustered, as shown by the spatial standard deviation ellipses.

The location of the equivalent dipole for a radially oriented cortical source patch (or here, effective sum of patches) is typically deeper than the cortical patch itself (Baillet et al., 2001). The equivalent dipoles for individual components in the P3b cluster (not shown) were scattered across parietal and central cortex (as indicated in Fig. 5 by its larger spatial standard deviation). Therefore, the equivalent dipole for the mean scalp map of the 'P3b' cluster (Fig. 6E-H) was unnaturally deep, thus representing the center of the active cortical source distribution only symbolically. The mean equivalent dipole location for the 'P3f' cluster (Fig. 6A-D) was estimated chiefly from the two periocular electrodes. Moreover, the complicated geometry of the frontal skull cannot be well fit to the spherical head model used here. Thus, its indicated mis-localization below the orbitofrontal brain surface should not be taken literally.

The spatial standard deviations of the other component cluster dipoles were smaller. Their equivalent dipoles indicate the respective dominant cortical regions of their source domains. Though the mean cluster scalp map for the central occipital alpha cluster (Cα) could be fit satisfactorily by a single equivalent dipole located in the central occiput, for several of the cluster components a better model of the component scalp map was obtained from a symmetric dipole pair in left and right peri-calcarine cortex (not shown).

3. Component cluster dynamics. Mean dynamics properties of nine non-artifact component clusters are summarized in Figs. 6-9 each of which shows the mean scalp map and response-locked ERP image, activity and ERP spectra, and ERSP for one or more component clusters. Because of the complexity of the results, we report and interpret the nine component clusters in four groups based on shared dynamic features.

3a. Two clusters contributing to the late positive response. Two component clusters made distinct contributions to the late positive complex of the target ERP:

Inferior frontal cluster (P3f). After subtracting the larger back-projected scalp data contributions of components accounting for blinks and saccadic eye movements, the response-locked ERP at both periocular channels contained a broad, circa 2-μV positive-going scalp potential peaking on average 39 ms before the recorded button press. Figure panels 6A-D show the mean scalp map and dynamic properties of a cluster of 10 independent components from 10 subjects that together largely accounted for an ERP feature whose time course was similar to the peak we labeled 'P3f' (for P3-frontal) in an earlier report on decomposing the matrix of 25 condition ERPs from these experiments (Makeig et al., 1999a). Note, in the ERP image (Fig. 6C), the absence of sharp excursions not regularly time-locked to experimental events, which would mark blinks or lateral eye movements. Such activity at far frontal and periocular channels was effectively separated out by ICA into artifact components (not shown). Instead, as shown in Fig. 6b, this component cluster accounted for nearly all the (P3f) positivity occurring before the button press, particularly in shorter latency-response trials (Fig. 6C).

Interpretation. The P3f cluster-mean response-locked positivity began near 150 ms, consistent with direct neurophysiological evidence that by 150 ms after stimulus onset, visual information is spread throughout the brain by a complex web of afferent and efferent connections (Klopp et al., 2000; Hupe et al., 2001). Subtracting the button travel time (~25 ms, roughly estimated from EMG recording during one experimental session) and the neuromuscular conduction time (~15 ms) suggested the P3f peak at 39 ms before the button press occurred very near the moment of the subcortical motor command. It is thus tempting to speculate that the P3f process should originate in frontal structures involved in motivated decision making and response selection, such as orbitofrontal cortex (Ikeda et al., 1996), though the sparse spatial sampling of the present data do not allow more specific conclusions.

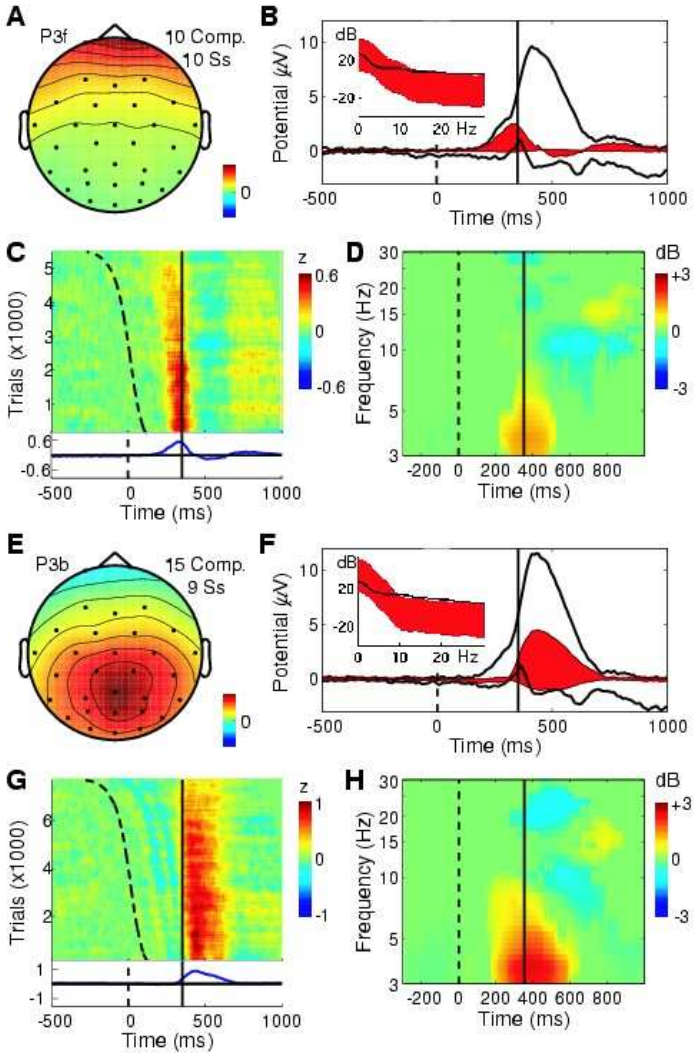

Figure 6. Far-frontal and parietal component clusters contributing to the P300. *Each set of four panels in Figures 6-9 shows: (A) The mean component scalp map. (B) The whole-data (black traces) and cluster-accounted (red filled) ERP envelopes (min and max voltage channel values at each time point), plus (inset) the power spectrum of the whole EEG (black traces) and the whole response-locked average ERP (red fill). The lower edge of the red fill shows actual ERP power, the upper edge, the phase-random EEG spectrum required to produce the observed average-ERP spectrum by phase cancellation. The difference between the upper edge of the red fill and the actual EEG spectrum (black trace) reflects phase consistencies across trials in the single trial data. (C) ERP-image plot of the color-coded single trials time locked to the response (solid vertical line) and sorted by response time from stimulus onset (dashed line). Trials normalized by dividing by the standard deviation of component activity in the 1-s pre-stimulus baseline. (D) The component mean ERSP showing mean event-related changes in (log) spectral power across data trials time locked to the response (solid line). Here, median stimulus delivery time is indicated by the dashed line. (Panels A-D) Far-frontal component cluster accounting for the pre-response (P3f) positivity. (Panels E-H) Broad parietal component cluster accounting for part of the post-response (P3b) positivity. The peri-response energy increase for these processes peaks at below 5 Hz.*

The far-frontal (P3f) component cluster response appears similar to the 280-ms 'P2a' peak noted in responses to (foveal) visual 'oddball' stimuli by Potts et al. (1998). Potts and Tucker (2001) reported that P2a was maximal near the eyes but can be recorded over most of the face and may also be found in attention conditions involving no subject button press. The scalp map of the ERP-derived 'P3f' component derived by ICA applied to the 25 condition ERPs (Makeig et al., 1999a) also included bilateral parietal features not seen here in the 'P3f' component cluster. Evidently, the temporal and far-

frontal projections joined in the ERP-derived P3f component map did not cohere in the much more extensive single-trial data and so were separated by ICA applied to the concatenated single-trial data. This detail points to the advantage of decomposing by ICA a sufficient number of unaveraged data trials over decomposition of even a relatively large set of averaged responses.

Central parietal cluster (P3b). Panels E-H of Fig. 6 show the mean scalp map and activity patterns of a bilaterally distributed cluster of 15 components (from 9 subjects) that projected most strongly to posterior and central scalp sites and made a substantial contribution to the slow post-motor 'P300' or 'P3b' positivity. Examination of the raw ERP waveforms of the six subjects not contributing to this cluster suggested the absence of a typical central parietal positivity in their target responses. The mean cluster scalp map (Fig. 6E) resembled that of the response-locked parietal ERP peak itself (Fig. 2B). The ERP image of the normalized single-trial component activity (Fig. 6G) includes an early series of small, positive and negative, wave fronts following the (sorted) time of stimulus delivery (*dashed curve*) by fixed delays. These are followed by a large response-locked positivity (*red area)* accounting for 62% of post-response ERP variance at 300 ms for site Pz. The P3b cluster positivity is clearly smaller in late-response trials (Fig. 6G, top), consistent with the Pz data (Fig. 2F). The mean cluster ERSP (Fig. 6H) reveals a significant (3-dB) post-response low-theta power increase.

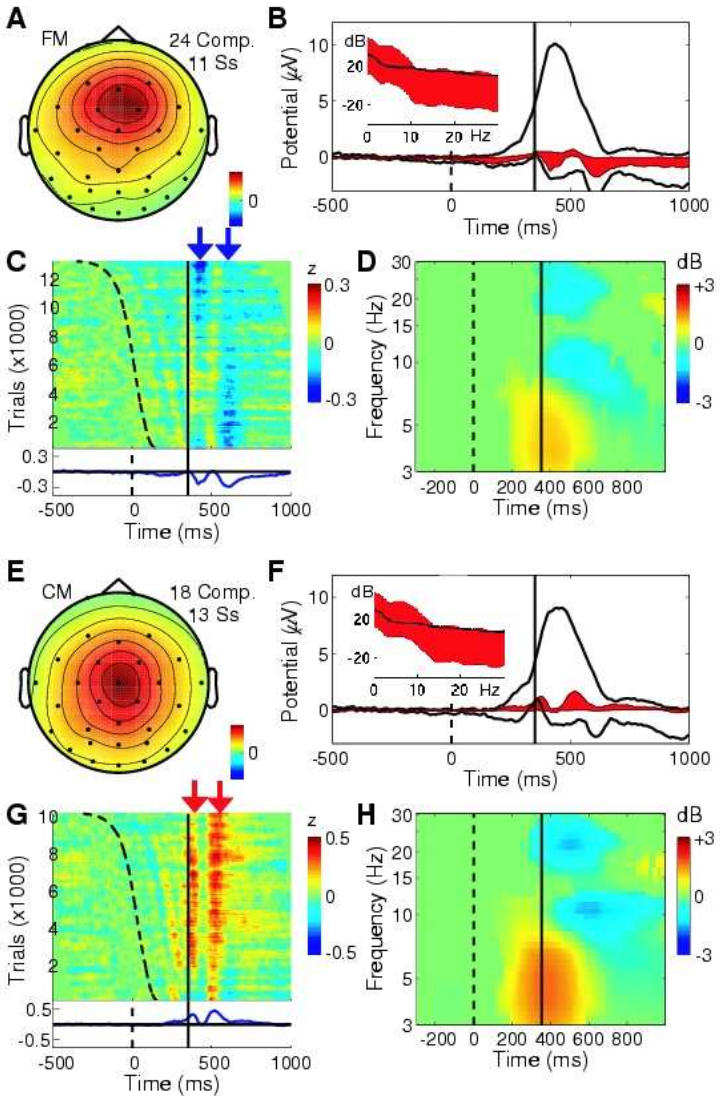

Figure 7. Two mediofrontal independent component clusters showing a post-motor theta response pattern. Panels as in Fig. 6. (A-D)Frontal midline (FM) cluster of components often exhibiting a theta-band peak in their activity spectra. E-H. Central midline (CM) component cluster projecting maximally to the vertex.

Intepretation. The significance of the stimulus-locked P300 (or 'P3b') peak over central parietal cortex has long been debated. Our results clearly show (Fig. 2E) that in these experiments this peak was time locked to and predominantly followed the motor response. P3b onset occurred at about the moment of the motor command, coincident with the P3f peak (see Fig. 10D). It could not, therefore, index activity involved in making the motor decision or action, as seemingly associated with the P3f process. The equivalent dipole distribution of the P3b cluster was broad, the strongest commonality being dipole orientation toward the central parietal scalp. Between-subject variability in locations of P3b generators have also been reported

by researchers using other source localization methods (Moores et al., 2003). It is possible that more advanced three-dimensional component clustering methods, applied to decompositions from more subjects and more data channels, might allow further distinctions among processes in this cluster.

3b. Central Midline Clusters. Figures 7 and 8 show mean properties of four classes of components producing the two-cycle post-response evoked-response pattern seen clearly in the response-locked data at site Fz (Fig. 2D). Principal among these were two component clusters (Fig. 7) projecting maximally to the frontal and central midline scalp, respectively.

In the RT-sorted frontal midline (FM) cluster ERP image (Fig. 7C), the two negative wave fronts follow the curving trace marking stimulus onsets, the second of these merging with the earlier RT-locked negativity. Though the vertex-maximum central midline component cluster (CM, Fig. 7E-H) also exhibited the post-motor theta feature (red arrows, Fig. 7F,G) with the mid frontal and mu rhythm clusters (see below), it contributed little to the broader (P3b) positivity produced mainly by the central parietal (Fig. 6E) and central occipital (Fig. 9E) component clusters.

Interpretation. Though the equivalent dipole locations of components in the two midline clusters were somewhat overlapping (Fig. 5), their mean equivalent dipole locations were generally consistent with sources in or near the dorsal anterior cingulate and cingulate motor areas, respectively (Ullsberger and von Cramon, 2003). These areas are implicated by fMRI and neurophysiological experiments as participating in motor response selection and anticipation of the consequences of events, including those involving self-perceived errors (Shima and Tanji, 1998; Luu and Tucker, 2001; Manthey et al., 2003; Ullsperger and von Cramon, 2003). The phase/latency of the post-motor theta burst appeared to be consistent across quicker and slower responses.

The theta burst appears to resemble other reported frontal midline EEG activity patterns: theta bursts or trains (fm) appearing during mental concentration (Mizuki et al., 1980; Gevins et al., 1997; Uchida et al., 2003) and brief bursts of theta activity linked to and following the error-related negativity (ERN) (Luu and Tucker, 2001; Luu et al., 2004), an ERP peak whose latency matches the first negativity in the FM-cluster post-response ERP (at ~60 ms). Inverse source modeling has placed the generating cortical domain of the ERN and fm in and/or near the dorsal anterior cingulate. In this ICA decomposition, however, the two-cycle post-motor theta burst pattern appeared not only in the frontal midline cluster, but also in the central midline, mu and parietal clusters (see below).

The scalp map of the central midline cluster (Fig. 7E) resembles scalp maps of the 'P3a' or 'P3novel' ERP peaks seen, for example, when unique and unexpected stimuli are included in a randomly alternating sequence of target and non-target stimuli (Courchesne et al., 1975; Polich and Comerchero, 2003). Here, however, the central midline cluster made only a small contribution to the stimulus-locked target ERP.

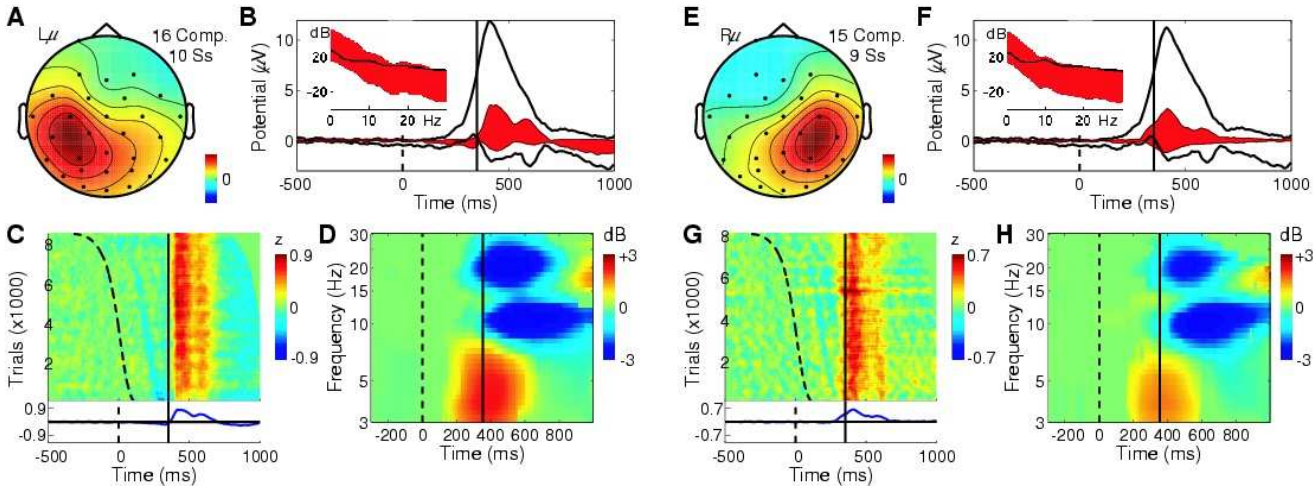

Figure 8. *Two mu-rhythm component clusters also showing the post-motor theta response pattern. Panels as in Fig. 6. (A-D) Left mu rhythm (Lμ) component cluster with mu characteristic 10-Hz and 22-Hz peaks in the activity spectrum. (D) Following the button press, this activity is blocked. (E-H) Corresponding right mu-rhythm (Rμ) component cluster.*

3c. Mu rhythm clusters. The left and right mu rhythm component clusters (Lμ and Rμ in Fig. 8) exhibited the defining features of mu rhythms – distinct spectral peaks near 10 Hz and 22 Hz that are strongly blocked following movements, with equivalent dipoles located roughly over hand motor cortex (and/or adjacent post-central somatosensory areas), and oriented roughly orthogonal to the directions of the central sulci. Both the ERP and ERSP peaks were larger in the left mu cluster (contralateral to the response hand) than in the right. In common with the midline clusters, the mu component clusters contained the two-cycle post-motor theta pattern (Fig. 8D) concurrent with a mean theta power increase (Fig. 8H). They also made slower, positive-going contributions to the parietal ERP, particularly to the late 'slow wave' phase of the stimulus-locked P300 complex that, unlike the main (P3b) peak, exhibits a polarity reversal over the central scalp (Simson et al., 1977).

Interpretation. In a previous ICA analysis of ERPs from these experiments, the late 'Slow Wave' phase of the stimulus-locked P300 complex was confined to a single component (Makeig et al., 1999a), but was here separated into distinct left and right mu rhythm processes in at least 10 of the subjects. More detailed source analysis of magnetoencephalographic (MEG) mu rhythms has assigned their source mainly to somatosensory cortex (Forss & Silen, 2001). Thus, the post-response slow positivity (Fig. 8C) of the Lμ cluster, larger following slower responses, might index tactile feedback from the hand and button surface (Makeig et al., 1999).

3d. Posterior alpha clusters. Figure 9 shows the dynamics of three clusters of components projecting to the posterior scalp. Each had a distinct near 10-Hz alpha frequency peak in their activity spectrum, most pronounced in components of the central cluster (Fig. 9F, *inset*). The stimulus-locked ERP contributions of the two lateral posterior alpha clusters, shown as sloping wave fronts in Fig. 9C,K and better shown in Figures 10G and 11C, included an early stimulus-locked peak accounting for most of the P1 ERP peak (near 145 ms), and for part of the succeeding N1 peak, which summed contributions from several clusters (cf. Fig. 10C,E,G). In the central alpha component cluster, the initial stimulus-locked response feature was followed by a train of circa 10-Hz stimulus-locked waves. These can be said to be produced

by partial phase resetting of the intermittent alpha activity of these components following stimulus onsets, since they were accompanied by *no* mean increase in alpha power. The central alpha cluster also made an appreciable broad, triangular contribution (Fig. 9F,G) to the P300 positivity, while the contributions of the lateral clusters to the response-locked ERP, beginning just before the button press, were small and narrow. The mean response-related ERSPs for these three clusters were weak (Fig. 9D,H,L), and their post-response alpha and beta blocking were brief and weak, compared to the two mu clusters (Fig. 8). The lateral clusters, but not the central cluster, exhibited a low beta increase above baseline (near 14 Hz) beginning near the button press.

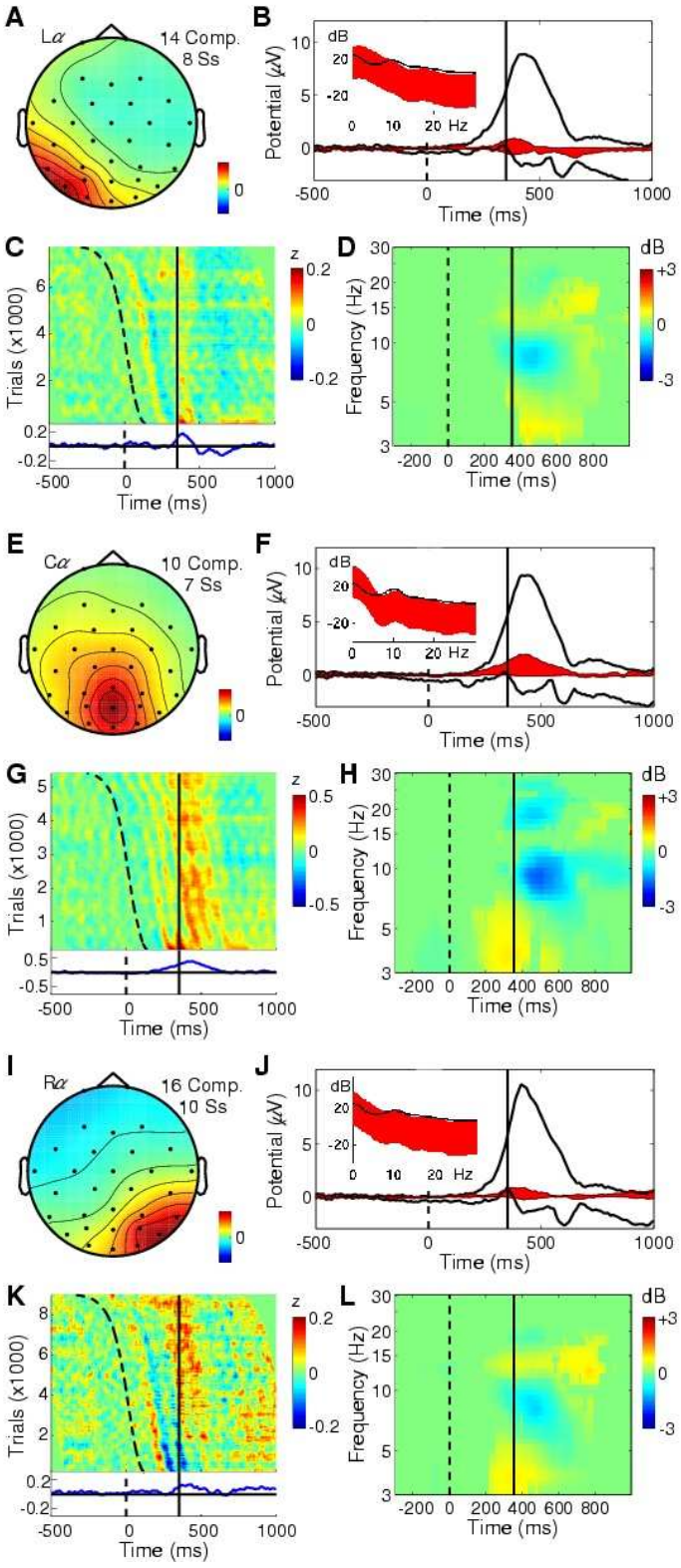

Figure 9. Three posterior alpha-rhythm component clusters*. Panels as in Fig. 6. (A-D) Left posterior alpha (Lα) component cluster. (E-H) Central posterior alpha (Cα) component cluster with characteristic trapezoidal scalp projection, consistent with a bilateral, peri-calcarine equivalent dipole source model, and contributing prolonged phase resetting following stimulus onset (curving dashed trace). (I-L) Right posterior alpha (Rα) component cluster. Note (C) the relative absence of the alpha-ringing pattern in the Lu cluster activity and the (D,H,L) relatively weak post-response alpha blocking in these clusters.*

Interpretation. While the existence of multiple alpha rhythms has long been noted, ICA here neatly separated their activities and identified their complete, overlapping scalp maps based on the relative independence of their activity patterns in the unaveraged data. The central-posterior alpha processes had a stronger alpha-band peak than lateral posterior alpha components, and showed longer-lasting phase resetting following visual stimulus onsets (Fig. 9G). The longer phase memory implied by the prolonged phase resetting is compatible with longer bursts of alpha activity in these components. Possibly, the distinct dynamics of the central and lateral posterior clusters may serve different though still unknown purposes.

The 'trapezoidal' signature of several of the central posterior component scalp maps (Fig. 9E) is compatible with a model comprising two equivalent dipoles located symmetrically in left and right peri-calcarine cortex. To be

fused into a single infomax ICA component, activity in both hemispheres must have been largely synchronous with negligible phase delay. Alpha-band activity in two cortical areas can indeed be synchronous if the two areas are densely connected, as here most likely via corpus callosum. Synchronization of bilateral generator regions via dense callosal coupling might also support the observed sharp (circa 10-dB) alpha peak in the activity spectra of these components.

In these data, the lateral posterior alpha components were always unilateral and never bilateral. Possibly this may reflect the lower density of direct connections between these areas. Early ERP features in these experiments appeared predominantly contralateral to the stimulus locations. No doubt this was because these stimuli were presented above and usually lateral to fixation. In other data, we have noted that visual ERPs time locked to foveally presented stimuli usually contain a bilateral posterior P1/N1/P2 complex (Makeig et al., in press).

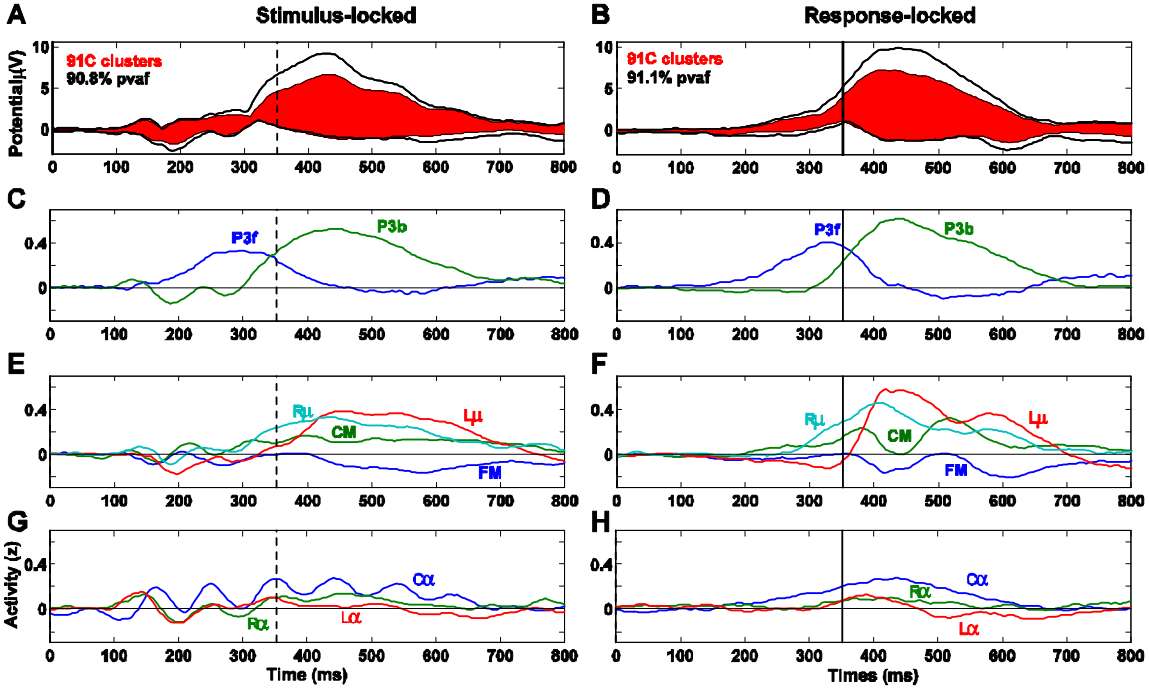

Figure 10. Component time courses and summed scalp projections. *Summed projections (A,B) to the grand-mean ERP average of all trials time-locked to stimulus onsets (left) and to subject responses (right), plus (C-H) grand mean normalized activity time courses of each of the nine independent component clusters, scaled and separated into the same cluster groupings as in Figs. 6-9. For comparison with the stimulus-locked responses (left), response-locked data epochs (right) are shown aligned to the mean subject-median response time (352 ms = dashed line in left panels).*

4. Component ERP contributions. Together, the nine component clusters accounted for 91.1% of the variance of the response-locked grand mean ERP at all channels in the 1000 ms following stimulus onset, as well as for 90.8% of the variance of the stimulus-locked grand mean ERP. Figure panels 10A and 10B show the envelopes (most positive and negative channel values, across all channels, at each time point) of the stimulus-locked and response-locked grand mean ERPs (*black*) and the (*red filled*) envelope of the summed back-projections to the scalp of the components comprising the nine clusters. The normalized grand average activity time courses for the nine clusters are shown in Fig. 10C-H for comparison with the time courses of the grand mean ERP (Fig. 10A,B).

Note that stimulus-locked component-cluster ERP activity first appeared in the lateral posterior alpha clusters (at 100 ms). Onset of the stimulus-locked ERP of the P3b cluster at about the same time was soon followed by the far-frontal P3f cluster onset (near 120 ms, Fig. 10C). The stimulus-locked ERP deflection began at the same moment in the four post-motor theta clusters (Fig. 10E). Six of the nine clusters had a negative peak in their stimulus-locked ERP average near 200 ms, confirming the spatial complexity of the N1 peak, as indicated by invasive measures (Klopp et al., 2000) and comparable to previous analysis of non-target epochs from this data set (Makeig et al., 2002a).

In the response-locked cluster ERPs, note that the P3f cluster activity appeared to begin early, while response-related activity in the P3b-cluster ERP diverged from baseline 10-20 ms before the P3f peak, concurrent with a posterior-negative peak in the left-mu cluster ERP. The posterior-positive peaks in the response-locked ERPs of both mu clusters, the early shoulder of the P3b-cluster ERP peak, the central-cluster ERP slow wave, and the negative-going peak of the FM cluster ERP all occurred together, about 100 ms after the P3f peak.

Figure 11 shows the individual and summed independent component cluster contributions to the grand mean ERP at sites Fz and Pz. At Pz, no component cluster contributed more than a third of peak parietal P300 amplitude in either the stimulus-locked or response-locked ERPs (Fig. 11C,D). The largest cluster contribution to the peak at Fz was also from the P3b cluster, which contributed about half its peak amplitude (Fig, 11A,B). The P3f cluster contributed at best a third. These results cast doubt on claims that the target-response P300 peak at Fz predominantly indexes frontal activity.

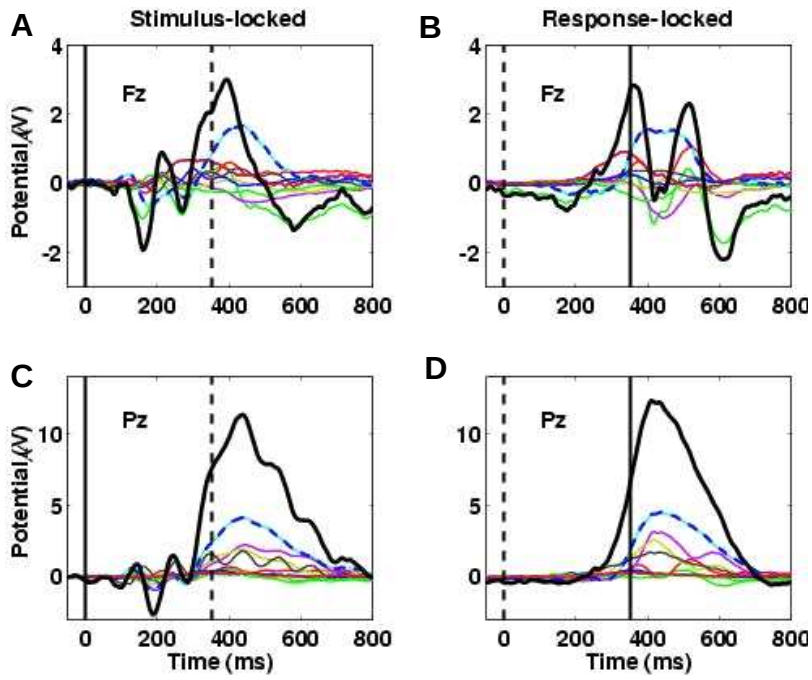

Figure 11. Cluster projections to the scalp ERP. *Component cluster contributions (in μV, thin traces) to the grand mean stimulus-locked and motor response-locked target ERPs at scalp sites Fz and Pz, plus their summed contributions (thick traces). Although the P3b cluster makes the largest contribution to the evoked responses at both scalp sites, its contribution does not outweigh the summed contributions of the other clusters.*

5. Post-response theta synchronization. Phase coherence analysis of consistent phase relationships between the frontal midline and central midline clusters, and between the frontal midline and left mu clusters, time locked to and following the motor response showed that significant theta phase coherence appeared in the data, even after the respective component ERPs were subtracted from each trial, indicating a transient post-response phase linkage between these otherwise maximally independent processes. Fig. 12 illustrates this phenomenon in the time domain using phase-sorted ERP-image plots. Sorting trials by the phase (with respect to the button press) of the post-motor theta activity of the frontal midline cluster (Fig. 12A) and then imaging the single-trial activities of the central midline cluster in the

same trial order (Fig. 12B), induced partial theta phase ordering on the center midline data (i.e., the slightly diagonal wave fronts in Fig. 12B). The converse procedure (Fig. 12C) gave a similar result (Fig. 12D).

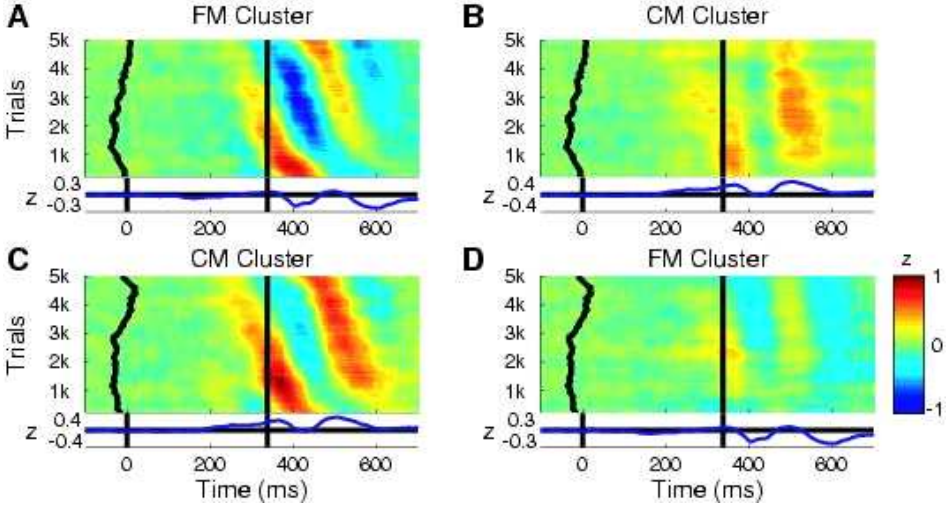

Figure 12. Phase-coupling of theta components: time-domain view. *(A) ERP-image view of baseline-normalized, response-aligned single-trial activity time series of components in the FM cluster, sorted (top-to-bottom) by phase at 4.87 Hz in a window centered 89 ms after the button press. Vertical smoothing: 400 trials. Units: μV normalized by dividing by the standard deviation of component single-trial baseline activity. The curving vertical trace (left) shows a moving-mean of stimulus onset times; the vertical line (central), the time of the button press. Data band pass in all panels: 0.1-40 Hz. (B) Exporting the same trial sorting order (from panel A) to CM cluster components (from the 9 subjects contributing components to both clusters) demonstrates the significant partial theta phase coherence (r~0.3) between the two clusters in the post-response time/frequency window. Note the induced (top-down, left-to-right) slope of the latency of the two (orange) positive-going CM-cluster theta wave fronts. (C) Phase-sorted ERP-image (as in panel A) of the normalized CM cluster trials. (D) FM-cluster component trials sorted in the same trial order as (C). Again, the partial theta-band phase coherence of the two clusters in the post-response period is reflected in the diagonal (blue) negative-going wave fronts of the FM cluster data.*

5. Post-response theta synchronization. Phase coherence analysis of consistent phase relationships between the frontal midline and central midline clusters, and between the frontal midline and left mu clusters, time locked to and following the motor response showed that significant theta phase coherence appeared in the data, even after the respective component ERPs were subtracted from each trial, indicating a transient post-response phase linkage between these otherwise maximally independent processes. Fig. 12 illustrates this phenomenon in the time domain using phase-sorted ERP-image plots. Sorting trials by the phase (with respect to the button press) of the post-motor theta activity of the frontal midline cluster (Fig. 12A) and then imaging the single-trial activities of the central midline cluster in the *same* trial order (Fig. 12B), induced partial theta phase ordering on the center midline data (i.e., the slightly diagonal wave fronts in Fig. 12B). The converse procedure (Fig. 12C) gave a similar result (Fig. 12D).

Visualizing theta dynamics. Figure 13 shows a single frame of an animation representing the joint response-related theta-band dynamics occurring in and between all nine component clusters. The figure shows an analysis window centered 89 ms after the button press. Note that the transient theta phase coherence between the mu, parietal and midline components was selective: phase coherence between FM and CM, FM and Lμ, and Rμ and P3b clusters (indicated by linking cylinders) were significant, whereas no significant phase linkage occurred in this time period between the FM and P3b clusters, nor between the CM and Lμ clusters. This selectivity diminishes the possibility that the observed transient phase linkages were produced by appearance of post-response EEG activity not separated out by ICA

into a separate component and therefore misattributed by the ICA model to nearby independent components. The results presented here, however, do not allow us to completely discount this possibility.

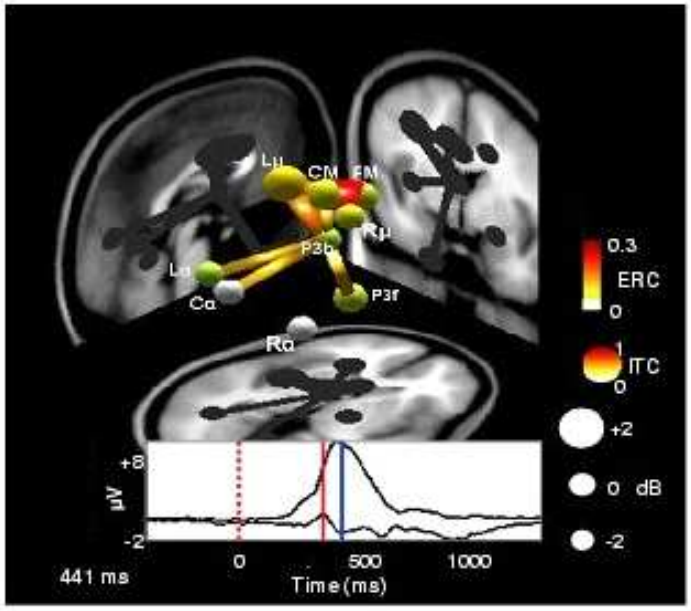

Figure 13. Post-motor theta dynamics. *Frame of an animation representing grand mean patterns of event-related dynamics in the theta band. Black traces in the lower panel show the envelope of the grand mean ERP time locked to the subject button press; (dotted vertical line) median time of stimulus onset (response-352 ms). Theta dynamics computed in a window (center frequency 4.87 Hz, 3-cycle Hanning taper) centered (blue vertical line) 89 ms after the button press (red vertical line). Each sphere in the upper panel represents the location of the equivalent dipole for a component cluster. Approximate projections of the equivalent-dipole locations are shown in shadow on three planes from an average MR image (Montreal Neurological Institute). Log spectral power changes (relative to pre-stimulus baseline) are indicated by the sizes of the spheres (see key, bottom right). Non-grey sphere colors indicate consistent inter-trial phase locking (ITC). Colored cylinders joining spheres indicate significant event-related phase coherence (ERC) between cluster components.*

Discussion

ICA used the temporal information contained in the single-trial EEG time courses to identify and separate maximally independent processes. These were associated with overlapping scalp maps and time courses whose distinctive features were no longer blurred by volume conduction as in the scalp electrode data. The nine independent component clusters here identified by their similar scalp projections and activity spectra resemble classes of EEG phenomena long described by neurologists from observation of paper data displays - central and lateral alpha, left and right mu, and frontal-midline theta rhythms. By cleanly separating the EEG contributions of these processes, ICA allowed exploration of their individual and joint event-related dynamics. Our finding of selective theta synchronization between frontal midline, motor and parietal processes (Fig. 13) was only possible using ICA. The clear separation of 'alpha-ringing' in the stimulus-locked response from the other ERP features (Fig. 10G) also illustrates the power of ICA to separate temporally and functionally distinct activities that are generated in different brain areas but project to the same scalp channels.

The nine clusters largely reproduced the component clusters we obtained previously from ICA decomposition of brief (100-ms) post-stimulus time windows following non-target and target stimuli in these experiments (Makeig et al., 2002a). The major difference in the two sets of clusters was the inclusion, here, of a parietal 'P3b' component cluster. In both analyses, the clustering omitted many small components with 'noisy' scalp maps and time courses, and also omitted 'outlier' components specific to single subjects. After removing clear ocular and muscle artifact components from the raw data, however, the nine identified EEG component clusters together accounted for over 90% of the

grand-mean ERP variance (over all channels) as well as almost 60% of variance in the whole EEG. By contrast, the ERP data themselves accounted for only 6% of post-stimulus EEG variance, supporting our claim that this analysis presents a more complete model of the event-related EEG dynamics occurring in these data than the average ERP.

Cluster localization. The group mean equivalent dipole locations shown in Fig. 5 only symbolize the actual distribution of the component source domains. The relation between processes derived by ICA from scalp data and processes seen in invasively recorded cortical data is not yet clear. For example, the equivalent dipole localization of the P3b cluster-mean scalp map does not correspond directly to all the cortical areas noted to generate P3b-like local field potentials in implanted pre-surgical epileptic patients by Halgren et al. (1995ab) -- parts of the superior parietal lobule, inferior frontal and temporal cortices, as well as the limbic medial temporal lobe. However, in general it is difficult to infer the cortical distribution of a cortical source domain from equivalent dipole location. Clearly, more inclusive methods of ICA component source localization fit to actual subject cortical geometry (Dale and Sereno, 1993) may be useful for further research. Conversely, however, it is not clear whether 'hot spots' recorded by sparsely implanted intracranial electrodes necessarily map activity that dominates the scalp EEG dynamics, which might arise from focal or more spatially diffuse activities in other areas.

Event-related spectral perturbations. Production of scalp EEG requires partial synchronies in local field activity extending across the relatively large (cm2 or more) domains of neuropile (Nunez, 1981). These must be dynamically maintained, and might well be perturbed by biological systems and mechanisms that implement and reinforce 'top-down' cognitive decisions such as, as here, to selectively attend and respond to relatively infrequent visual stimuli while ignoring frequent non-targets (Giesbrecht et al., 2003). Posterior alpha, in particular, increases promptly when visual attention shifts between hemifields or between visual auditory stimulus streams (Worden et al., 2000). Most of the spectral perturbations appearing in this analysis have been previously reported in some form, for instance the alpha blocking following visual stimuli cueing visual attention and mu-blocking accompanying cued finger movements (Hari et al., 1997; Pfurtscheller et al., 2000). A late beta increase following target responses has also been reported (e.g., Makeig, 1993).

ERP influence. Traditionally, averaging event-locked EEG data from single scalp channels to form an ERP is assumed to reject, by random phase cancellation, 'background' EEG rhythms whose statistics are tacitly assumed to be unaffected by experimental events. To test the effect of the average ERP on the observed spectral perturbations, we computed the cluster ERSPs again after removing the component mean ERP from each trial (not shown). All the effects shown in Figs. 6-9 remained significant.

Common ERSP features. Note that many of the cluster ERSPs (Figs. 6-9) share common features. How is this possible? First, 'independent' components returned by infomax decomposition of EEG data are never perfectly independent, but are instead those found by infomax to be maximally independent. This is not a mere play on words, but an advantageous feature of infomax decomposition that allows it to separate activity from different cortical areas even when the independence of synchronous activities within those areas is not unbroken or absolute. Second, the infomax independence metric is weighted toward separation by phase differences rather than by power spectral differences. The observed spectral perturbations may reflect, in part, common modulatory influences of central neurotransmitter-labeled brainstem systems involved in orienting and arousal, which project widely to cortex and are known to

change the spectral properties of cortical field activity following novel or meaningful events (Fries et al., 2001; Hasselmo et al., 2002; Aston-Jones et al., 2001).

Functional significance of the post-motor theta bursts. At and after the button press, a mean fronto-central theta power increase appeared in all 15 subjects' data. It was partially phase-coherent in four of the component clusters and was not eliminated by removing the subject-mean ERP from each trial. Local bursts of theta band-activity are widely distributed on the human cortex (Kahana et al. 1999) and associated with cognitive function (Caplan et al., 2003). In hippocampus, an association between theta phase and high-frequency 'sharp wave' activity has been observed in animals (Csicsvari et al., 2003). In turn, high frequency activity can index organization of spike timing of similarly-tuned neurons into brief near-synchronous volleys more likely to trigger further spikes in common target neurons (Fries et al., 2001; Salinas & Sejnowski, 2002).

Following non-target stimuli in this experiment, frontal midline components exhibited weak 'theta-ringing' (partial post-stimulus theta phase locking) not accompanied by increased theta power (Makeig et al., 2002a). Here, following targets a two-cycle period of increased theta activity appeared, time-locked to the motor response and weakly phase coherent between midline frontal, parietal and motor areas. Coherent theta activity might enhance the speed, salience, and reliability of spike-based communication between these and other brain areas connected with them, including hippocampus and related limbic structures including amygdala (Seidenbacher et al., 2003). The result might be facilitation of information transfer about the event and its anticipated consequences to and from memory structures, and selective retuning of attentional states in relevant cortical areas based on anticipatory evaluation of the consequences of the cued motor response, including readjusted sensory and motor expectancies.

The post-motor theta bursts seen here following correct speeded responses very likely are tightly linked to the ERP feature with strong theta-band energy that follows highly speeded manual (or foot) responses in the Erickson flanker task (Holroyd et al., 1995). Luu and Tucker (2001) have suggested that the so-called error-related negativity (ERN) in the response-locked ERP following responses the subject knows immediately to be in error partly represents partial phase-locking of transiently increased theta-band activity in frontal midline and other sources (Luu, Tucker and Makeig, in press). A similar negative-going ERP feature has been reported following negative feedback whose valence is not known in advance (Ruchsow et al., 2002; Gehring and Willoughby, 2002). Luu and Tucker (2001) also reported the appearance of enhanced theta activity in the ERP above somatomotor cortex following known-error responses. Our animation of event-related theta band dynamics in our data (Fig. 13) demonstrates that correct speeded button presses produce partially synchronized theta-band increases in frontal (but not central) medial and contralateral somatomotor process clusters. Mean coherence phase lag between the midline clusters suggested that the post-motor theta activity in the frontal midline cluster components lead that of central midline components by about 8 ms, a physiologically plausible value whose statistical reliability should be tested on a larger data set.

Post-motor theta and P300. Elbert and Rockstroh (1987) have proposed that cortical surface positivities in general index periods of relative neural depolarization and concomitant insensitivity ('disfacilitation') of the involved cortex to distal input, possibly explaining the concurrent attentional blink (McArthur et al., 1999; Kranczioch et al., 2003) and amplitude decrease in the auditory steady-state response (Rockstroh et al., 1996). Von Stein et al. (2001), on the other hand, have reported that following delivery

of visual targets to cats, coherence in the theta band occurred between the output layer of a higher and the input layer of a lower visual cortical area. They did not observe this coherence following non-target stimuli. Thus, the post-motor P300 and the theta burst response may have complementary functions: to decrease 'bottom-up' environmental sensitivity and to concurrently apply the results of 'top-down' processing to cortical perceptual areas. Although probably not available for observation in scalp data, the post-motor theta-band synchronization might extend to limbic areas (hippocampus, amygdala, etc.) and play a role in memory updating (e.g., of learned/remembered 'context') following goal-directed actions (cf. Seidenbecher et al., 2003). Thus, we suggest that the post-motor theta burst may reflect directly the 'context-updating' processes previously proposed to be indexed by the broad P300 positivity (Dien et al., 2003).

Evoked responses. In this speeded response paradigm at least, the ERP 'P300' positivity was near-strictly time locked to and predominantly followed the motor response. The 'P300' positivity was, here, indeed a late positive complex of potentials generated in several brain areas, confirming results of invasive recording (Smith et al., 1990) and clinical group-difference studies (Potts et al., 1998). ICA decomposed the unaveraged EEG signals summing to the target-response ERP into event-related activity into several classes of brain EEG processes originating predominantly in frontal, central, parietal and occipital cortex. This result adds to longstanding doubts about the specificity of ERP peak measures. In particular, it shows that parietal sources may account for less than half of the peak amplitude of the stimulus-locked positive peak at Pz (Fig. 11C), the most commonly used index of 'P300' magnitude. Altogether, we found four component clusters contributing to the P300 maximum at Pz -- in descending order, central parietal, left and right mu, and central occipital alpha EEG processes. As well, the (threefold) largest EEG contributor to the stimulus-locked P300 positivity at Fz is volume-conducted from the same parietal (P3b cluster) sources, casting strong doubt on the specificity of peak amplitude at Fz for indexing frontal function.

Phase resetting. As in our previous single-trial analysis of some of these data (Makeig et al., 2002a), partial phase resetting of ongoing intermittent alpha and theta EEG processes contributes to some features of the average ERP. However, partial phase resetting is not a sufficient model for all the ERP features. For example, the central posterior alpha cluster actually showed a post-motor response decrease in alpha power during its prolonged 'alpha ringing' ERP contribution (Fig. 9G,H), whereas the monopolar parietal 'P300' ('P3b'') ERP feature was associated with an event-related increase in both whole EEG variance in the central parietal channel (Pz) (not shown) and in component activity variance of the P3b, Ca and Lμ clusters that contributed the most to it.

The central posterior 'alpha ringing' feature of the stimulus-locked ERP can be parsimoniously described as arising through alpha phase resetting. The P300/P3b feature, on the other hand, might better conform to the usual conception of an ERP as measuring evoked response activity added to ongoing EEG activity. Note in Fig. 6H, however, that the low-frequency energy of the P3b cluster component activities increased by less than 3 dB at 3 Hz, demonstrating that the 'baseline' activity of these processes included slow-wave processes with similar spectral characteristics. The post-motor theta burst phenomenon composed both a frequency specific power increase and significant (though partial) phase-locking through its two-cycle ERP duration.

The variety of these ERP features suggests that assuming a strict dichotomy between 'evoked' and 'phase-reset' activities is unproductive. Rather, each ERP feature may be usefully and better

characterized as summing event-related perturbations of various sorts in the ongoing activities of one or more localized cortical EEG processes. To produce a reproducible peak or peaks in the average ERP, these perturbations should involve some degree of (partial) phase locking of the contributing process activities to the time-locking events in one or more frequency regions. At very low (near-DC) frequencies, event-related 'phase locking' implies event-related 'sign locking.' For example, the 'P300' would never appear in ERP averages at all if it were negative-going in half the trials. Similarly, there need be no strong dichotomy between 'evoked' phenomena that involve partial phase locking and so contribute to average ERPs, and 'induced' phenomena that may involve changes in spectral amplitudes but do not show phase locking and thus do not contribute to average ERPs. Rather, it is important to realize that most event-related EEG dynamics have both 'induced' and 'evoked' aspects.

Event-related brain dynamics. The results presented here confirm that extensive, complex and flexible information concerning links between cognitive processes and macroscopic brain dynamics are available in non-invasive high-density EEG data. Availability of more comprehensive analysis techniques, such as introduced here, should make EEG (and related magnetoencephalographic, MEG) data analysis of increasing interest both to cognitive neuroscientists and to neurophysiologists, as event-related EEG dynamic models complement observations of slow-changing hemodynamics while greatly expanding the restricted spatial information available from single- and multi-neuron spike recordings.

References

Ardekani B, Choi S, Hossein-Zadeh GA, Porjesz B, Tanabe JL, et al. (2002) Functional magnetic resonance imaging of brain activity in the visual oddball task. Brain Res Cogn Brain Res 14(3): 347-356.

Amari S (1998) Natural gradient works efficiently in learning, Neural Computation, 10: 251-276.

Anemueller J, Sejnowski TJ, Makeig S (2003) Complex independent component analysis of frequency domain electroencephalographic data. Neural Networks 16, 1311-1323.

Aston-Jones G, Chen S, Zhu Y, Oshinsky ML (2001) A neural circuit for circadian regulation of arousal. Nat Neurosci 4(7): 732-738.

Baillet S, Mosher JC, Leahy RM (2001) Electromagnetic brain mapping. Sig Proc Mag, IEEE, 18:14-30.

Bell AJ, Sejnowski TJ (1995) An information-maximization approach to blind separation and blind deconvolution, Neural Computation 7:1129-1159.

Caplan JB, Madsen JR, Schulze-Bonhage A, Aschenbrenner-Scheibe R, Newman EL, et al. (2003) Human theta oscillations related to sensorimotor integration and spatial learning. J Neurosci 23(11):4726-36.

Courchesne E, Hillyard SA, Galambos R (1975) Stimulus novelty, task relevance and the visual evoked potential in man. Electroencephalogr Clin Neurophysiol 39:131-143.

Cover TM, Thomas JA (1991) Elements of Information Theory. New York: John Wiley. 542 p.

Csicsvari J, Jamieson B, Wise K, Buzsaki G (2003) Mechanisms of gamma oscillations in the hippocampus of the behaving rat. Neuron 23(2):311-22.

Dale AM, Sereno MI (1993) Improved localization of cortical activity by combining EEG and MEG with MRI cortical surface reconstruction: A linear approach. J Cogn. Neurosci. 5:162-176

Delorme A, Makeig S, Fabre-Thorpe M, Sejnowki, TJ (2003) From single-trial EEG to brain area dynamics, Neurocomputing 44-46: 1057-1064.

Delorme A, Makeig S (2004a) EEGLAB: MATLAB toolbox for electrophysiological data analysis. Institute for Neural Computation, University of California San Diego. Available: http://www.cnl.salk.edu/~scott/ica.html via the Internet. Accessed 2004 Feb 10.

Delorme A, Makeig S (2004b) EEGLAB: An open-source toolbox for analysis of EEG dynamics. J Neurosci Methods, 134:9-21.

Dien J, Spencer KM, Donchin E (2003) Localization of the event-related potential novelty response as defined by principal components analysis. Brain Res Cogn Brain Res 17(3):637-50.

Ebmeier KP, Steele JD, MacKenzie DM, O'Carroll RE, Kydd RR, et al. (1995) Cognitive brain potentials and regional cerebral blood flow equivalents during two- and three-sound auditory "oddball tasks." Electroencephalogr Clin Neurophysiol 95:434-443.

Elbert T, Rockstroh B (1987) Threshold regulation - a key to the understanding of the combined dynamics of EEG and event-related potentials. J Psychophysiolog 4:317-333.

Enghoff S (1999) Moving ICA and time-frequency analysis in event-related EEG studies of selective attention. Technical Report INC-9902. Institute for Neural Computation, University of California San Diego, La Jolla CA.

Ford JM, Sullivan EV, Marsh L, White PM, Lim KO, et al. (1994) A The relationship between P300 amplitude and regional gray matter volumes depends upon the attentional system engaged. Electroencephalogr Clin Neurophysiol 90:214-228.

Forss N, Silen T (2001) Temporal organization of cerebral events: neuromagnetic studies of the sensorimotor system. Rev Neurol (Paris) 157 (8-9 Pt 1), 816-821.

Frei E, Gamma A, Pascual-Marqui R, Lehmann D, Hell D et al. (2001) Localization of MDMA-induced brain activity in healthy volunteers using low resolution brain electromagnetic tomography (LORETA). Hum Brain Mapp 14: 152-165.

Fries P, Reynolds J, Rorie A, Desimone R (2001) Modulation of Oscillatory Neuronal Synchronization by Selective Visual Attention. Science 291(5508):1560-63.

Giesbrecht B, Woldorff MG, Song AW, Mangun GR (2003) Neural mechanisms of top-down control during spatial and feature attention. NeuroImage 19:496-512.

Gehring WJ, Willoughby AR (2002) The medial frontal cortex and the rapid processing of monetary gains and losses. Science 295 (5563), 2279-2282.

Gevins A, Smith ME, McEvoy L, Yu D (1997) High-resolution EEG mapping of cortical activation related to working memory: effects of task difficulty, type of processing, and practice. Cerebral Cortex 7(4): 374-85.

Halgren E, Squires NK, Wilson CL, Rohrbaugh JW, Babb TL, et al. (1980) Endogenous potentials generated in the human hippocampal formation and amygdala by infrequent events. Science 210:803-805.

Halgren E, Baudena P, Clarke JM, Heit G, Liegeois C, et al. (1995a) Intracerebral potentials to rare target and distractor auditory and visual stimuli. I: Superior temporal plane and parietal lobe. Electroencephalograp. Clin Neurophysiol 94: 191-220.

Halgren E, Baudena P, Clarke JM, Heit G, Marinkovic, K (1995b) Intracerebral potentials to rare target and distractor auditory and visual stimuli. II: Medial, lateral and posterior temporal lobe. Electroencephalogr Clin Neurophysiol 94: 229-250.

Hari R, Salmelin R, Makela JP, Salenius S, Helle M, et al. (1997) Magnetoencephalographic cortical rhythms. Int J Psychophysiol 26(1-3): 51-62.

Hasselmo M, Hay J, Ilun M, Gorchetchnikov A (2002) Neuromodulation, theta rhythm and rat spatial navigation. Neural Networks 15: 689-707.

Holroyd CB, Dien J, Coles MG (1998) Error-related scalp potentials elicited by hand and foot movements: evidence for an output-independent error-processing system in humans. Neurosci Lett. 242:65-8.

Hupe J-M, James A, Girard, P, Lomber SG, Dayne BR, et al. (2001) Feedback connections act on the early part of the responses in monkey visual cortex. J Neurophysiol 85(1): 134-45.

Ikeda A, Luders HO, Collura TF, Burgess RC, Morris HN, et al. (1996). Subdural potentials at orbitofrontal and mesial prefrontal areas accompanying anticipation and decision making in humans: a comparison with Bereitschaftspotential. Electroencephalogr Clin Neurophysiol 98((3): 206-12.

Jung, T-P, Makeig S, Humphries C, Lee TW, McKeown MJ, et al. (2000a) Removing electroencephalographic artifacts by blind source separation. Psychophysiol 37(2): 163-78.

Jung T.-P, Makeig S, Westerfield M, Townsend J, Courchesne E, et al. (2000b) Removal of eye activity artifacts from visual event-related potentials in normal and clinical subjects. Clin Neurophysiol 111: 1745-58.

Jung T-P, Makeig S, McKeown MJ, Bell AJ, Lee T-W, et al. (2001a) Imaging Brain Dynamics Using Independent Component Analysis. Proc IEEE 89(7): 1107-22.

Jung TP, Makeig S, Westerfield M, Townsend J, Courchesne E et al. (2001b) Analysis and visualization of single-trial event-related potentials. Hum Brain Mapp 14(3):166-85.

Kahana MJ, Sekuler R, Caplan JO, Kirschen M, Madsen JR, et al. (1999) Human theta oscillations exhibit task dependence during virtual maze navigation. Nature 399(6738): 781-4.

Klopp J, Marinkovic K, Chauvel P, Nenov V, Halgren E (2000) Early widespread cortical distribution of coherent fusiform face selective activity. Human Brain Mapping 11:286-93.

Knight RT, Scabini D, Woods DL, Clayworth CC (1989) Contributions of temporal-parietal junction to the human auditory P3. Brain Res 502:109-116.

Kranczioch C, Debener S, Engel AK (2003) Event-related potential correlates of the attentional blink phenomenon. Cogn Brain Res 17:177-87.

Luu P, Tucker DM (2001) Regulating action: alternating activation of midline frontal and motor cortical networks. Clin Neurophysiol 112: 1295-306.

Luu P, Tucker D, Makeig S (2004) Frontal midline theta and the error-related negativity: Neurophysiological mechanisms of action regulation. Psychophysiology, in press.

McArthur G, Budd T, Michie D (1999) The attentional blink and P300. Neuroreport 10(17): 3691-5.

Makeig S (1993) Auditory event-related dynamics of the EEG spectrum and effects of exposure to tones. Electroencephalogr Clin Neurophysiol 86: 283-93.

Makeig S, Bell AJ, Jung T-P, Sejnowski TJ (1996a) Independent component analysis of electroencephalographic data. In: Touretzky D, Mozer M, Hasselmo M, editors. Advances in Neural Information Processing Systems 8. Cambridge, MA: MIT Press, pp. 145-151.

Makeig S, Jung T-P, Ghahremani D, Sejnowski TJ (1996b) Independent component analysis of simulated ERP data. Technical Report INC-9606. Institute for Neural Computation, University of California San Diego, La Jolla CA.

Makeig S, Jung T-P, Ghahremani D, Bell AJ, Sejnowski TJ (1997) Blind separation of auditory event-related brain responses into independent components. Proc Natl Acad Sci USA 94:10979-10984.

Makeig S, Westerfield M, Jung T-P, Covngton J, Townsend J, et al. (1999a) Functionally independent components of the late positive event-related potential during visual spatial attention. J Neurosci 19: 2665-80.

Makeig S, Westerfield M, Townsend J, Jung T-P, Courchesne E (1999b) Functionally independent components of early event-related potentials in a visual spatial attention task. Phil Trans Royal Soc London B Biol Sci 354(1387): 1135-1144.

Makeig S, Westerfield M, Jung T-P, Enghoff S, Townsend J (2002a) Dynamic brain sources of visual evoked responses. Science 295(5555): 690-93.

Makeig S, Debener S, Onton J, Delorme A (2004) Mining event-related brain dynamics. Trends Cogn Sci, in press.

Manthey S, Schubotz RL, von Cramon DY (2003) Premotor cortex in observing erroneous action: an fMRI study. Brain Res Cogn Brain Res 15(3): 296-307.

Mizuki Y, Tanaka M, Isozaki H, Nishijama H, Inanaga K, et al. (1980) Periodic appearance of theta rhythm in the frontal midline area during performance of a mental task.Electroencephalogr Clin Neurophysiol 49: 345-351.

Moores K, Clark C, Hadfield JL, Brown GC, Taylor DJ (2003) Investigating the generators of the scalp recorded visuo-verbal P300 using cortically constrained source localization. Hum Brain Mapp 18(1): 53-77.

Nunez P (1981) Electric Fields of the Brain: the Neurophysics of EEG. New York: Wiley. 484 p.

Pfurtscheller G, Aranibar A (1977). Event-related cortical desynchronization detected by power measurements of scalp EEG. Electroencephalogr Clin Neurophysiolog 42: 817-826.

Pfurtscheller G, Neuper C, Krausz G (2000) Functional dissociation of lower and upper frequency mu rhythms in relation to voluntary limb movement. Clinical Neurophysiology 111(10): 1873-9.

Polich J, Comerchero M (2003). P3a from visual stimuli: typicality, task, and topography. Brain Topogr 15: 141-52.

Potts G, Hirayasu Y, O'Donnell BF, Shenton ME, McCarley RW (1998). High-density recording and topographic analysis of the auditory oddball event-related potential in patients with schizophrenia. Biol Psychiatr 15: 982-989.

Potts G, Tucker DM (2001) Frontal evaluation and posterior representation in target detection. Brain Res Cogn Brain Res 11(1): 147-56.

Rockstroh B, Muller M Heinz A, Wagner M, Berg D, et al. (1996) Modulation of auditory responses during oddball tasks. Biol Psychol 43(1): 41-55.

Ruchkin DS, Johnson R, Canoune HL, Ritter W, Hammer M (1990) Multiple sources of P3b associated with different types of information. Pychophysiol 27:157-176.

Ruchsow M, Grothe J, Spitzer M, Kiefer M (2002) Human anterior cingulate cortex is activated by negative feedback: evidence from event-related potentials in a guessing task. Neurosci Lett. 14:203-6.

Salinas E, Sejnowski TJ (2001) Correlated neuronal activity and the flow of neural information. Nat Rev Neurosci 2(8): 539-50.

Seidenbecher T, Laxmi TR, Stork O, Paper H-C (2003) Amygdalar and hippocampal theta rhythm synchronization during fear memory retrieval. Science 301:846-850.

Shima K, Tanji J (1998) Role for cingulate motor area cells in voluntary movement selection based on reward. Science 282(5392): 1335-8.

Simson R, Vaughn HG, Ritter W (1977) The scalp topography of potentials in auditory and visual Go/Nogo tasks. Electroencephalogr Clin Neurophysiol 43:864-875.

Smith ME, Halgren E, Sokouk M, Gaudena P, Musolino A (1990) The intracranial topography of the P3 event-related potential elicited during auditory oddball. Electroencephalogr Clin Neurophysiol 76(3): 235-248.

Soltani M, Knight R (2001) Neural origins of the P300. Crit Rev Neurobiol 14(3-4): 199-224.

Sutton S, Braren M, Zubin J, John ER (1965) Evoked-potential correlates of stimulus uncertainty. Science 150:1187-1188.

Townsend J, Courchesne E. (1994) Parietal damage and narrow "spotlight" spatial attention. J Cogn Neurosci 6(3), 220-232.

Uchida S, Maehara T, Hirai N, Kawa K, Shimizu H, et al. (2003) Theta oscillation in the anterior cingulate and beta-1 oscillation in the medial temporal cortices: a human case report. J Clin Neurosci 10(3): 371-4.

Ullsperger M, Von Cramon DY (2003) Error monitoring using external feedback: specific roles of the habenular complex, the reward system, and the cingulate motor area revealed by functional magnetic resonance imaging. J Neurosci 23(10): 4308-14.

von Stein A, Chiang C, Konig P (2000) Top-down processing mediated by interareal synchronization. Proc Nat Acad Sci USA 97:14748-14753.

Worden MS, Foxe JJ, Wang N, Simpson GV (2000) Anticipatory biasing of visuospatial attention indexed by retinotopically specific alpha-band electroencephalography increases over occipital cortex. J Neurosci Online 20(6): RC63.